International Journal of Thermodynamics (IJoT)
ISSN 1301-9724 / e-ISSN 2146-1511
www.ijoticat.com

Vol. 22 (No. 4), pp. 193-201, 2019
doi: 10.5541/ijot.639634
Published online: December 1, 2019

Simple Refrigerating Device for Multiparametric Analysis of the Thermoacoustic Cooling – Design, Assembly and Testing of the Setup

Authors: K. Grzywnowicz[1]*, L. Remiorz[2]

Silesian University of Technology, Department of Power Engineering and Turbomachinery
ul. Konarskiego 18A, 44-100 Gliwice, Poland
E-mail: [1]krzysztof.grzywnowicz@polsl.pl,[2]leszek.remiorz@polsl.pl

Received 29 October 2019, Revised 22 November 2019, Accepted 22 November 2019

Abstract

Although the widespread introduction of numerical tools and the CFD models have improved the design methodology of thermoacoustic coolers and eased optimization of such units, high computational costs vitally limit their application in parametric analyses of thermoacoustic devices. Thus, experimental investigation remains essential field of research, considering design of such units. In the paper, the design and construction of an experimental setup, dedicated to perform an extensive multiparametric analyses on compact thermoacoustic devices with varying characteristic parameters, is discussed in detail. A complete design path, beginning with general consideration, with further detailed dimensioning and selection of market-available parts, ending with installation of control and data acquisition equipment, is described. Initial testing of the device, performed both computationally at the design stage and experimentally after the final setup assembling, is discussed as well. The results of the tests demonstrated ability to observe the variability in the operational parameters of the cooler following change in number of environmental and constructional parameters. The data acquired indicated vital importance of the stack porosity and frequency of the acoustic wave on performance of the thermoacoustic device, which corresponds to the data presented in the literature.

Keywords: *Thermoacoustics; experimental setup; multiparametric analysis.*

1. Introduction

Heat transfer from a low-temperature source to a high-temperature sink, taking place in refrigerators, is commonly realized using mechanically-driven compressors, which increase the pressure of a refrigerant gas in conventional compressor-based units. Alternatively, in order to reduce the technical and operational limitations that are linked with the use of a compressor, systems transporting liquid solution of the working medium, in the form of absorption systems, are used as well. However, in order to reduce the complexity of installations, thermoacoustic devices, utilizing oscillating pulses of acoustic pressure, have also been used in a number of cases.

Over the last twenty years, there have been a number of trials of the construction of devices that performed the role of either a thermoacoustic cooler or a heat pump [1,2,3]. Such devices appear as an alternative to the classical cycles for numerous reasons. The most important among them are: utilization of environmentally inert working fluids (mainly noble gases and their mixtures), possibility of achieving low temperatures with simple designs and consumption of energy in the form of either electricity or high-temperature heat (i.e. hot exhaust gases). Furthermore, the maintenance advantages, as the lack of sliding seals and no requirement for lubricants, as well as possibility of using traditional transducers (such as membrane loudspeakers) due to low pressure ratios might be listed as well [4,5]. Simultaneously, simplicity of the construction of thermoacoustic devices could result in both low manufacturing and maintenance costs.

The basic thermoacoustic unit comprises five basic elements (Figure 1.), including: a regenerative heat exchanger (named 'regenerator' or 'stack'), hot and cold heat exchangers, a covering tube (often called a 'resonator'), and a source of acoustic waves, which is commonly a traditional electro-acoustic transducer. The stack might be made of a porous material (i.e. set of parallel plates or sheets of a thin solid rolled up into a spiral), mainly ceramics or steel wool. The resonator might incorporate a classical tube or complex shapes, such as a Helmholtz resonator, in order to minimize the internal losses. Nevertheless, in number of cases, more sophisticated units (Figure 2.) are used. They differ from the simplest ones primarily by the resonator, equipped with an elliptical branch, called an acoustic loop, and a thermal buffer.

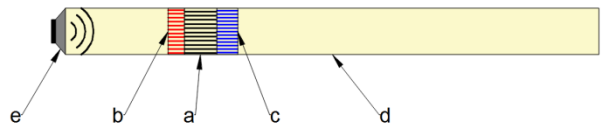

Figure 1. Diagram of a thermoacoustic device: a - the stack, b - hot heat exchanger, c - cold heat exchanger, d - the resonator, e – the source of the acoustic wave (Figure is in color in the on-line version of the paper).

Pressure oscillations, following the propagation of an acoustic wave emitted by i.e. a membrane loudspeaker, leads to the spatially limited motion of the working medium within the stack and its surroundings. Part of the working

*Corresponding Author

gas is pushed towards the warmer heat exchanger, and the rest is pulled back to the colder part of the setup. Due to the direct connection between temperature and pressure, introduced with the equation of state, oscillatory changes take place in the local temperature of the medium. Furthermore, direct thermal contact between part of the moving gas and the walls of the stack, enclosing the pores where the gas moves in, results in heat transfer on the solid-fluid boundary.

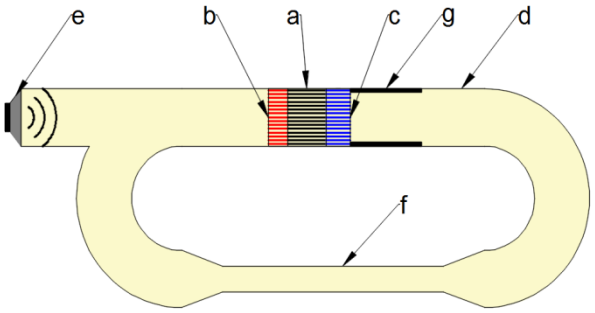

Figure 2. Diagram of the device with an acoustic loop: a - the stack, b - hot heat exchanger, c - cold heat exchanger, d - the resonator, e - source of the acoustic wave , f – acoustic loop, g – thermal buffer (Figure is in color in the on-line version of the paper).

Such interaction might be described by specific thermodynamic cycle, tending to the either Stirling or Brayton cycle, depending on the conditions of the acoustic wave's propagation [3,4] (Figure 3.). As a result of the interaction, heat transfer from the source of lower temperature to the environment characterized by a higher temperature occurs.

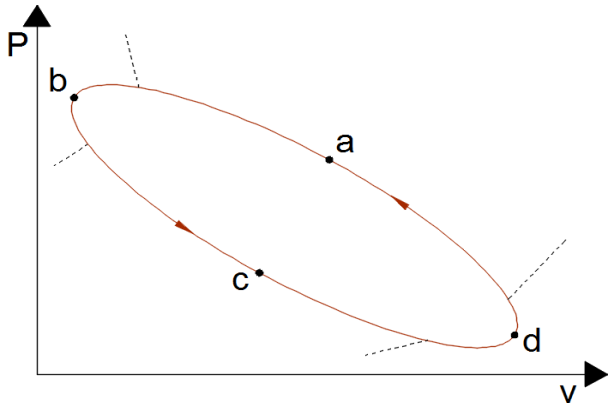

Figure 3. Thermodynamic cycle of the standing-wave thermoacoustic cooler/heat pump: a) movement of the gas towards the pressure antinode and its compression, b) heat rejection into the stack, c) movement of the gas towards the pressure node and its expansion, d) heat absorption from the stack [6].

According to the up-to-date knowledge, thermoacoustic devices have emerged as a promising field of modern cryogenic technology [2]. Their application would possibly introduce a new quality to numerous applications in emergency medicine, waste management, or the chemical or food industry [2,7,8]. A vital issue, influencing the widespread implementation of thermoacoustic installations in the future, is an increase in their operational parameters, enabling them to compete with traditional, commercially mature technology. Although computational techniques are increasingly being used in the design and optimization field of the aforementioned devices [9], experimental investigation remains crucial for solving vital challenges in the design of sophisticated installations [10,11]. However, availability of works considering complete preparation of experimental setup for testing of compact thermoacoustic refrigerators, from the initial design consideration up to final assembling level, is strongly limited. In the paper, a complete design path, supported by results of numerical simulations and simples experimental testing, with profound discussion on material processing and data acquisition challenges, is described.

2. Strategy for Design of Simple Thermoacoustic Cooler

2.1 Fundamental Concepts

The essential parameter, describing the efficiency of any cooling device, is the coefficient of performance (COP). Considering thermoacoustic units, in general, the characteristic curves of the available power and the COP are divergent [3,12,13]. Thus, design of the refrigerating units is focused on either maximization of their cooling power or their COP. This presents a complex issue, which can be resolved using numerical analyses. Nevertheless, the introduction of the fundamental rules of design, based on the linear theory of thermoacoustic devices, enables achievement of beneficial compromise to be achieved for the introductory design of a simple unit.

Due to its importance for the overall operational parameters of the final device, the design of a thermoacoustic cooler should begin with the consideration of the geometry and material of the stack. The theoretical expressions, describing how the acoustic power is used within the stack are complicated [1,3,7,14,15]. Thus, the simplified expressions deduced from the short stack and the boundary-layer approximations are commonly used instead [13,16]. The assumptions, linked with the aforementioned approximations, introduce the conditions of a large acoustic wavelength (much larger than the stack length). This condition allows to consider the pressure and the velocity constant over the discussed heat exchanger. Furthermore, the assumption of temperature difference across the stack is low enough to assume that the thermophysical properties of the working medium are constant [1,17]. For an easier description of the thermal and viscous phenomena, taking place at the interface between the gas and the stack material, the thermal and viscous penetration depths, defined by Eqs. (1)-(2), respectively, are introduced.

$$\delta_a = \sqrt{\frac{2K}{\omega \rho c_P}} \tag{1}$$

$$\delta_v = \sqrt{\frac{2\mu}{\omega \rho}} \tag{2}$$

In order to simplify the calculations, number of dimensionless parameters, essential for a profound analysis of the thermal-acoustic phenomena, is commonly introduced as well [1,3,5]. One of the most important is stack porosity, defined as the ratio of the cross-sectional area occupied by the working gas and the total cross-sectional area of the stack, given by Eq. (3) [1,4,18].

$$B = \frac{A_{st,w}}{A_{st,w}+A_{st,s}} \tag{3}$$

Proper design of the stack, considering its porosity and internal cross-sectional shape, requires initial identification of the working medium's parameters, including its mean gauge pressure and dynamic pressure amplitudes. Effective power, in the form of heat flux of a thermoacoustic cooler, vitally rises with the mean pressure of the medium. However, high pressure results in a small optimal stack spacing, causing vital difficulties during manufacturing and assembly of the exchanger [1,19]. In most common cases, the mean pressure of the working gases in compact devices does not exceed 10 bar [1,20]. The amplitude of the dynamic pressure, and therefore the pressure impulse inducing the thermoacoustic phenomenon, is limited by nonlinear effects which take place at the entrance and within the pores of the stack. Furthermore, it might be vitally affected by the operational parameters of the source (such as the maximal voltage or the coil's inductivity) as well. Considering the number of compact devices, pressure amplitudes are usually set within the range of 3-5 percent of the mean gauge pressure of the working gas [1,3,20].

The essential features of the assumed stack geometry are its porosity, which value should not fall below 0.6 to avoid high acoustic losses, and its hydraulic radius. Although number of stack geometries have been discussed recently [3,18,19], circular pores (Figure 4. variant "a"), parallel plates (Figure 4. variant "b"), and the pin array have been deemed as the best solution in the majority of compact units [1,18].

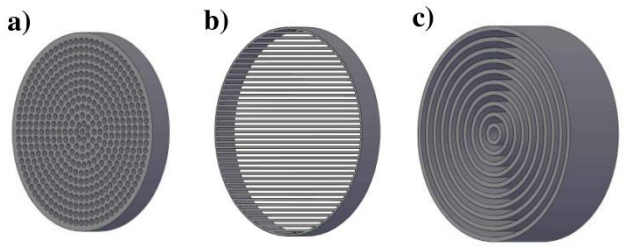

Figure 4. Common types of stack: a – circular pores, b – parallel plates, c – concentric cylinders.

In order to limit the acoustic losses at the perpendicular planes inside the resonator, both hot and cold heat exchangers should be characterized with geometry similar to that of the geometry of the stack. However, the relative lengths of these exchangers have to be optimized according to the properties of the working medium and the acoustic conditions [1,3].

The dynamic pressure and frequency of the sound wave are the most significant acoustic conditions in the device [1,20,21]. Since, in the case of simple standing-wave units, the frequency depends on the geometry of the resonator, its length should be equal to a half or a quarter of the wavelength of the sound wave [1,3]. This condition has to be fulfilled to maintain acoustic resonance inside the acoustic canal (Figure 5.). Its cross-sectional shape should be designed on the basis of the losses criterion, which directly depends on the friction between the canal surface and the working medium [1,3,21]. Thus quarter-of-a-wavelength resonators are preferable [1,3]. Furthermore, acoustic friction losses might be further reduced by using resonators with a discontinuous cross-section [1]. The length of respective heat exchangers, extracting waste heat to ambient or deriving heat from the refrigerated cavity, are determined by the distance of the heat transfer in the working gas [1,18] during a single oscillation. This length basically corresponds to the average peak-to-peak displacement of its portion at the location of the exchangers, as given by Eq. (4).

$$x_D = \frac{2 \cdot p_d}{\rho a^2 \omega} \sin(kx) \tag{4}$$

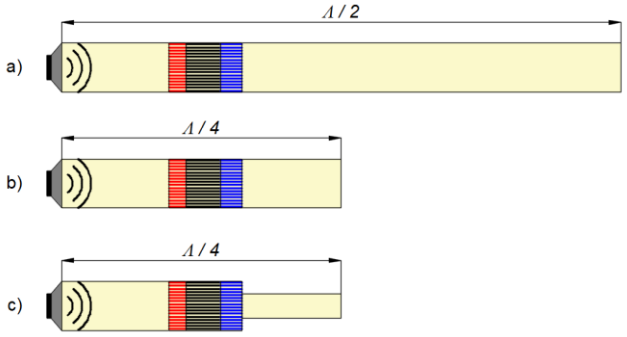

Figure 5. Common geometries of cylindrical resonators: a - half-wavelength, b - quarter-wavelength, c - quarter-wavelength with discontinuous diameter (Figure is in color in the on-line version of the paper).

As a general rule, a hot heat exchanger has to be longer than a cold exchanger, since it dissipates a greater heat flux [22,23]. Nevertheless, the appropriate design of all the elements of a thermoacoustic unit, including their proper interaction between each other, dictates the matter of optimization [3,14,19]. This process is commonly performed using genetic algorithms or the particle swarm and similarly sophisticated optimization techniques [14,19,24,25]. Furthermore, optimization currently might utilize the computational fluid dynamics (CFD) tools as well [1,3,26]. Use of such environment enables accurate identification of both temperature and pressure distributions, essential for reducing the thermal and viscous losses i.e. inside the heat exchangers [1,3,26]. Nevertheless, their utilization is coupled with high computational costs and the long periods of time that are required to perform a more sophisticated investigation. Thus, simplified numerical models, derived from the fundamentals of acoustics and heat transfer are often used as well [1]. Despite the vital simplifications, these models are suitable for basic optimization of simple units, such as single-stack standing-wave thermoacoustic coolers, and the preliminary investigation of more complex installations [1,19,23,27,28].

2.2 Design of an Experimental Device

The experimental setup, dedicated to perform the investigation of thermoacoustic refrigerators, consisted of several fundamental parts, including: data acquisition and control equipment, an isolated pressure vessel and a controllable thermoacoustic device. The issue of essential importance is the consideration of the design of a setup enabling precise control of a large number of vital parameters that affect its operational state.

To further simplify assembly of the setup, especially considering the automation and control system, an uniformly cylindrical geometry of the acoustic canal was assumed. To reduce the inherent viscous losses at the solid-fluid boundary within the canal, the length of the resonator was assumed to be a quarter of the resonant wavelength. The requirement for the minimization of external heat losses and the maximization of the mechanical properties of

the canal resulted in the selection of (poly)acryl being used to manufacture the resonator tube. The performance of measurements under the conditions of variable pressure frequency oscillations was enabled by the introduction of a movable closing wall, made from polyvinyl chloride (PVC). Since the device was designed to operate over a variety of frequencies, the range of its value needed to be assumed first. The acoustic frequency range is basically limited by the peak of the viscous losses and the frequency response of the loudspeaker used as a sound source. Commonly, wide-range flat loudspeakers of intermediate diameters operate at frequencies ranging from 300 to 10000Hz [21]. However, such membrane speakers are commonly characterized by a non-linear sound pressure level (SPL) versus frequency curve, with a low-frequency power peak corresponding to a value between 500-800Hz [29]. Thus, for further consideration, an average operational frequency of 600Hz was assumed. The maximal operating pressure of the working gas in the laboratory-scale devices was assumed to be equal to 10bar. Discussed assumptions essentially affected the design of the control volume, how the device should be moved during the experiments, and partially determined the geometry of the regenerator [1,14].

Dimensions of the stack pores are dependent on the cross-sectional area required to decrease the peak velocities of the working medium, as well as the satisfactory internal area of the fluid-solid boundary interface. The number and hydraulic radius of the pores, applied in the stack, have to correspond to the assumed porosity, as they directly affect the acoustic power transformation within the stack [1,18]. However, the optimal dimensions are limited by the available manufacturing technology and its pricing, since the geometry of neighboring heat exchangers should be similar to that of the stack [17,21]. Due to the intensive development of rapid prototyping technologies, including the stereolitography (SLA), vital drop in stack manufacturing costs has been observed. Thus, three-dimensional printing techniques seem to have become most beneficial in the case of low- and medium-temperature devices. Moreover, a number of materials, commonly used in the rapid prototyping, is characterized by beneficial thermophysical properties, i.e. low thermal conductivity (as approximately 0.16 W/(m•K) for acrylonitryl-butadiene styrene [30]). Design of the stack geometry was proceeded by ensuring its high efficiency and considering the available manufacturing technology of the subsequent exchangers. Thus, the regenerator in the setup was assumed to have a 57 mm diameter cylinder with pre-drilled cylindrical openings of 1.2 mm diameter, corresponding to thin drill bits for automatic production systems. In order to enable production of the element using classical numerical control machining, the offset between subsequent pores was assumed to be roughly equal to two thirds of the drill's diameter. This assumption resulted in the regenerator characterized by 406 non-uniformly arranged drills (Figure 6. variant "a") with a volume porosity of 45.8% [21].

In order to enable sophisticated loss analysis, the exchanger was set to be manufactured with variable porosity and a gas-solid interfacial area density. Thus, the other stack, characterized by a volume porosity of 14.4%, was prepared as well (Figure 6. variant "b"), comprising 25 pre-drilled openings of 3.8 mm diameter [21].

The geometry of neighboring heat exchangers was designed to correspond to the shape and location of the internal pores of the stack, in order to minimize losses at the stack-exchanger boundary. Detailed consideration for the geometry was based on the requirement for the handling mass of the replaceable stack in order to shorten the time required for its exchange between subsequent experiments.

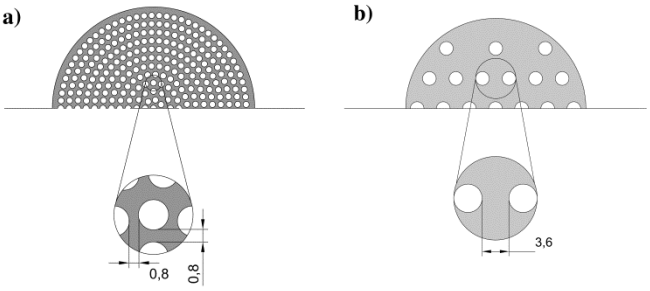

Figure 6. Cross-sectional geometry of a stack with: a) high porosity, b) low porosity [21].

Nevertheless, since the test-stand had to enable investigation under conditions of variable pressure and working medium composition, a set of exchangers was located within the sealed pressure vessel. This fact introduced extreme difficulties in the connection of the external circulating working medium. Therefore, the ambient gas was assumed to be the source and the sink of the external thermal energy for the operation of the cold and hot exchangers [21]. To meet the stated conditions, the heat exchangers were manufactured from copper alloy in the form of double-sided flanges (Figure 7.).

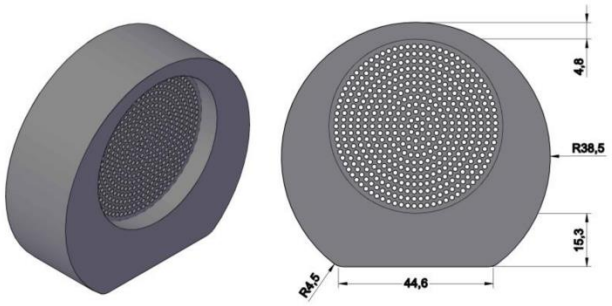

Figure 7. Geometry of the designed hot and cold heat exchangers [21].

In order to perform precise dimensioning of the assumed geometry of the exchangers, detailed consideration of the previously introduced parameters of the resonator and the speaker was required. The internal diameter of the flange, forming the exchanger, had to fit the external diameter of the stack. Simultaneously, the diameter of the flange had to correspond to the diameter of the acoustic canal, limited i.e. by the sizing of the commercially available flat membrane speakers of the requisite output powers. Therefore, the final design of the resonator had to be coupled with the choice of the acoustic transducer. Following the consideration, the setup was equipped with an acrylic pipe of 60mm external diameter and 2.5mm wall thickness, performing the role of the resonator. As a transducer, the flat membrane speaker of 57mm mounting diameter (54mm diameter of the diaphragm) and a maximum acoustic power of 2W [21,29] was assumed. Since the resonator was closed at one of its ends with a movable stiff wall to induce the acoustic resonance, the thickness of the wall was assumed to be a value of 3 mm. The value has been chosen to satisfy the condition of stiffness, which was essential to obtain the

acoustic resonance inside the canal. In order to simplify the problem of changing its relative position, the utilization of a stepper motor coupled with threaded bar stock was assumed (Figure 8.). The discussed solution consisted of permanently mounted stiff wall, fixed to the bushing by single screw and a gasket, with threaded bar stock screwed into the bushing on one side and connected to the stepper motor on the other side. The essential joint between the bar stock and the bushing was obtained using two blocking screws and an adhesive (Figure 9.).

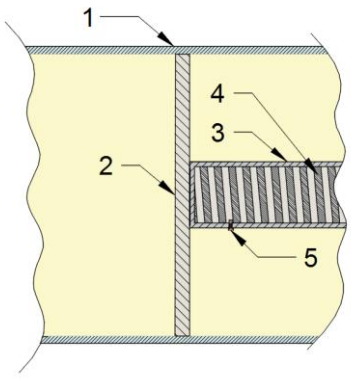

Figure 8. Diagram of the movable stiff wall unit: 1 – resonator, 2 – stiff PVC wall, 3 – bushing, 4 – threaded bar stock, 5 – blocking screw (Figure is in color in the on-line version of the paper).

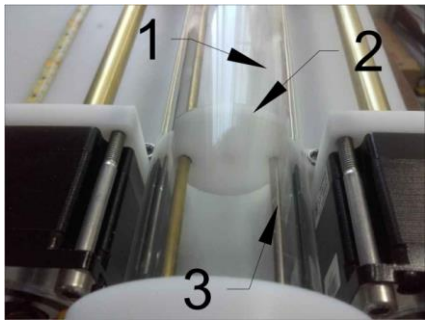

Figure 9. Photograph of the movable stiff wall unit: 1 – resonator, 2 – stiff PVC wall, 3 – bushing (Figure is in color in the on-line version of the paper).

The stepper motor of the stiff wall was connected to the programmable microcontroller via a conventional RTU485 protocol, which enabled automated control of its motion at 300 different movement commands or on a manual setting. A similar solution was applied to the movable speaker holder, being a proposed solution for the relative positioning of the heat exchangers along the axis of the device. However, in order to prevent blockage of the speaker inside the canal, i.e. due to quick accidental angular positioning of the setup, a motor with high power and stability was used. In order to prevent further damage to the movable elements, caused by an internal error of the program or an inappropriate manual setting, two position limit sensors were mounted in the setup and interconnected with the respective microcontrollers. The sensors were located on the edge of the resonator (to control the movement of the stiff wall) and the speaker mounting cover (to control the movement of the speaker). Further control of the design parameters of the unit, especially considering the geometrical properties of the regenerator, was introduced by the movable basis of the heat exchangers, allowing for the implementation of stacks of varying length (in the range from 20 to 30 mm). Parameters of the thermoacoustic device might vitally depend on the mean pressure and the composition of the working medium. Thus, to enable performance of pressure tests of up to 5bar gauge pressure, the resonator was unsealed and the setup was located in a certified pressure vessel (Figure 10. and Figure 11.). A static pressure sensor, which enabled measurement of up to 6bar relative pressure at a stable accuracy of 0.5%, was mounted inside the vessel cavity, above the acoustic canal. A compact microphone, performing the role of an acoustic pressure sensor, was mounted to the common base of the experimental setup on a movable base joint. To enable independent measurements of pressure and frequency control, the microphone was mounted on a bushing, crossing the closing stiff wall via a pre-drilled hole. Both pressure sensors were interconnected with normalizing pressure transducers. Additionally, a traditional gauge manometer, capable of measuring pressures of up to 10bar, was installed at the inlet of the pressure vessel.

Figure 10. Pressure vessel connected to the external source of working medium (Figure is in color in the on-line version of the paper).

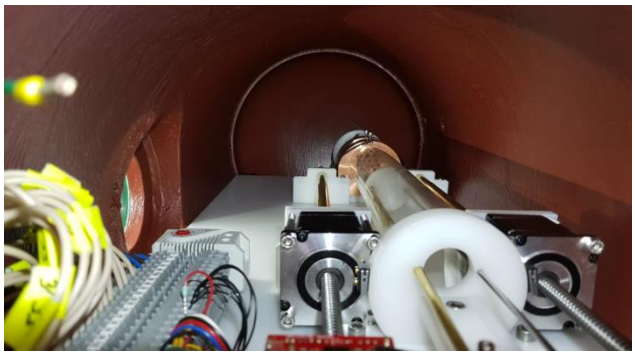

Figure 11. Internal cavity of the pressure vessel (Figure is in color in the on-line version of the paper).

As the temperature sensors, the five double-wired Pt100 resistance thermal devices (RTD), characterized by measurement uncertainty below 0.25°C, were implemented within the setup. The sensors were located on the speaker membrane's plane and at the dynamic pressure sensor, at the external surfaces of the exchangers (in the middle plane of both the hot and cold heat exchangers, 3±1 mm from the respective external wall surfaces) and in the free pressure vessel's volume. All the listed RTDs listed were connected to the common data acquisition card, normalizing the outputs and transmitting the acquired data via the RTU485 bus. Additionally, in order to control the average temperature of the working medium, the setup was equipped with a temperature control unit, located at the

bottom of the setup base. The unit consisted of a digital microcontroller, an electric heater with a 100W heating power and an external forced convection fan, which was interconnected with the manually operated temperature controller.

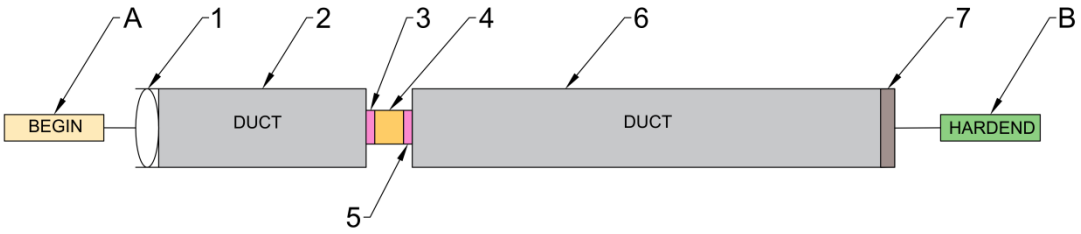

Figure 12. Diagram of the computational model of the unit in the DeltaEC™ environment: 1 – electroacoustic transducer, 2 – part of the resonator, 3 – hot heat exchanger, 4 – stack, 5 – cold heat exchanger, 8 – the rest of the resonator, 7 – closing stiff wall, A – set of initial conditions and boundary conditions for the transducer, B – set of boundary conditions for the closing wall (Figure is in color in the on-line version of the paper).

3. Computational and Experimental Tests of the Device

3.1 Methodology and Testing Procedure

In order to verify the general operational parameters of the setup, as well as to identify any potential fundamental errors in its design, numerical analysis of the unit was performed. The computations were performed using the dedicated DeltaEC™ software, which is commonly used tool for numerical research of thermoacoustic units [1,3,14,19,23]. Despite the fact that a number of simplifications were introduced, the software utilizes a simple and reliable linear model of thermoacoustic devices, deriving important data in a number of cases, as proven in the literature [1,22,31]. In order to use the discussed software, first, a mathematical model of the setup (Figure 12.) was prepared.

The model consisted of a total number of seven functional elements, with two additional blocks of boundary conditions and seven additional segments of algebraic dependences, dedicated to perform more sophisticated calculations. The functional elements, in order of appearance, included: the electroacoustic transducer unit, part of the acoustic canal located near to the transducer, the hot heat exchanger, the stack, the cold heat exchanger, part of the acoustic canal located near to the closing wall and the closing wall.

Additional blocks of equations was used to enforce local suppression of acoustic resistance and the energy flux at the closing wall in order to maintain acoustic resonance inside the resonator. Furthermore, these blocks of equations derived the set of general initial conditions, defined for the investigated unit, as well as part of boundary conditions referring to the electroacoustic transducer. The remaining blocks were defined in order to enable automatic performance of more sophisticated computation, including the temperature difference between the hot and cold heat exchangers, as well as the thermal and acoustic power, transferred through the control volume.

Numerical analysis of the unit was performed for five different acoustic frequencies, corresponding to total length of the resonator, which were equal to 250 mm, 300 mm, 350 mm, 400 mm and 450 mm. Each case was simulated for two different stack porosities, corresponding to the properties of the regenerator manufactured during the setup assembly.

Numerical simulation of the unit was executed by numerical integration of the differential equations of: momentum, energy conservation and the acoustic wave, defined for respective segments of the model indicated in Figure 12. The integration was performed using the explicit Runge-Kutta ("RK4") algorithm within the DeltaEC™ environment [32].

In order to validate the proper operation of the setup, initial testing was performed. Furthermore, performed testing enabled identification of the ability to perform parametric analyses with the installed equipment and decreased the risk of malfunction of the core thermoacoustic device. The tests focused on the investigation of the change in the temperature of the cold and hot heat exchangers, under the variable frequency of the acoustic wave, corresponding to different lengths of the acoustic canal. Subsequent lengths, assumed to be 400mm and 300mm, were ensured by locating the movable stiff wall at the respective positions. Experiments were performed for two low-porous stacks, made from ABS (acrylonitrile-butadiene styrene) and steel wool, respectively, using dry ambient air at atmospheric pressure, at initial temperatures of 25°C and 26°C (with ±0.5°C tolerance) for the respective measurement series. The amplitude of the dynamic pressure oscillations, that enforced the thermoacoustic phenomenon, did not exceed 350Pa [29]. This value was limited by the construction and the operational features of the membrane loudspeaker installed within the setup. Due to the preliminary character of this research, no thermal loads were put on hot and cold heat exchangers.

The measurement schedule, which was assumed for the test, included measurements of the temperature every 60 seconds from the start of the acoustic wave emission, with the last measurement taken twelve minutes after initialization.

3.2 Results and Discussion

The results of the simulation, concerning the obtained heat exchangers temperature difference, are indicated in Figure 13.

The results of the computational investigation demonstrated the essential dependence of the constructional feature of the regenerative heat exchanger on the primary effect of the thermoacoustic phenomenon, which was investigated in the setup at no-load state. The temperature difference between subsequent exchangers, in the case of the high porosity stack, acquired a value approximately

nine times greater than in the case of low porosity stack. Furthermore, in both cases, the values of the observed difference decreased with the increasing length of the resonator, which might correspond to increasing losses along the internal walls of the acoustic canal.

The data, collected during the experimental testing of the unit, is presented in Figure 14a. and Figure 14b. for the first series of measurements, corresponding to a 22mm long stack made from ABS. The results of the second series of measurements, corresponding to a 30mm long stack made from steel wool, are presented in Figure 15a. and Figure 15b. for different lengths of the acoustic canal, respectively.

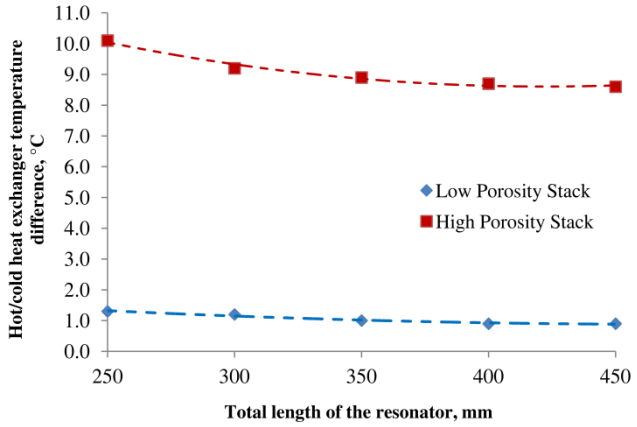

Figure 13. Results of the computational simulation of the unit. Low porosity stack corresponds to 14.4% stack porosity. High porosity stack corresponds to 40.5% stack porosity.

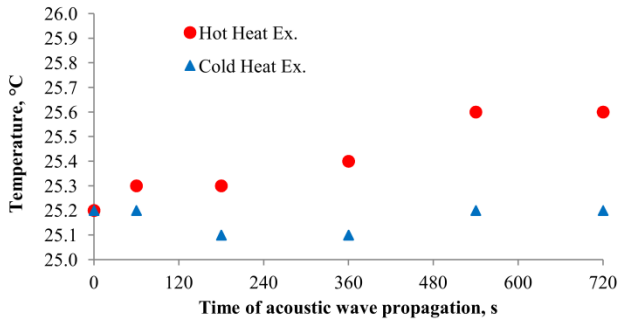

Figure 14a. Results of the measurements for a 400mm long acoustic canal with a 22 mm long ABS regenerator.

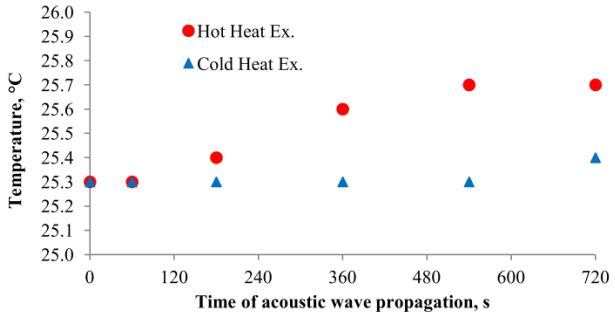

Figure 14b. Results of the measurements for a 300mm long acoustic canal with a 22 mm long ABS regenerator.

Considering the experimental results, the change in acquired values were comparable with the results obtained for low-power units, presented in the literature [20]. Nevertheless, the stable temperature of the cold heat exchanger, visible in the Figure 14b., might have been caused by the excessive influence of heat transfer from the ambient volume with a higher temperature. This suggests requirement for utilization of thermal insulation for longer measurement series.

The similar stability of the temperature of the hot heat exchanger, visible in Figure 15a., might have had the effect of significant heat dissipation through conduction by the steel wires that formed the steel wool stack.

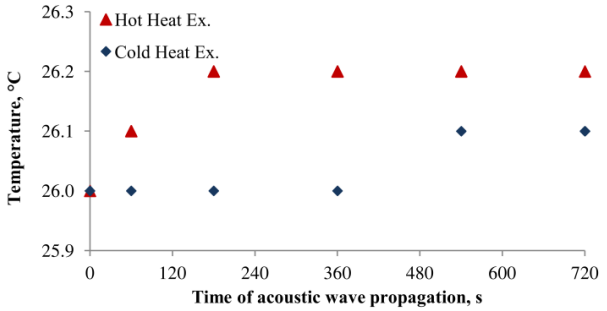

Figure 15a. Results of the measurements for a 400mm long acoustic canal with a 30 mm long steel regenerator.

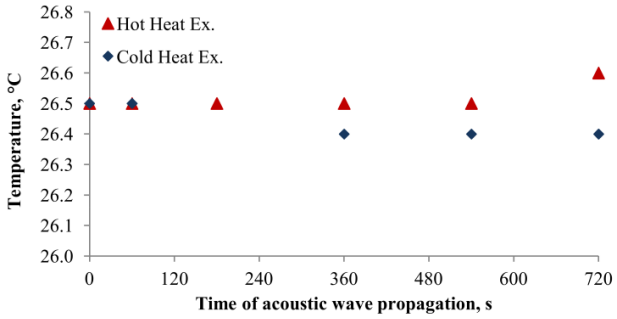

Figure 15b. Results of the measurements for a 300mm long acoustic canal with a 30 mm long steel regenerator. Singular coarse error visible.

This is supported by the sudden rise in the cold heat exchanger's temperature, observed at 600 and 720 seconds. The sudden drop in the cold heat exchanger's temperature, observed during the tests for the 300mm long resonator case, was identified as an internal error of the measuring unit's equipment. Therefore, this particular measurement was not considered as valid within the series. Furthermore, temperature measurement uncertainty at relatively high level might also contributed to observed error, as well as influenced short-time temperature stabilization, visible in the Figure 14b. and the Figure 15b. Nevertheless, considering the mentioned investigation, the temperatures remained stable until the final time step of the analysis, where a difference at the level of 0.2°C between the subsequent exchangers was visible. This might be influenced by the large losses in the low-porosity wool stack, increasing with the rise in the frequency of the acoustic wave emitted by the speaker, following the decrease in total length of the acoustic canal.

Nevertheless, the experimental results correspond for the data obtained from the numerical simulation. As

indicated in Figure 13., for the stack of low porosity, the temperature difference among hot and cold exchangers did not exceed 1.2°C, with vital drop following rise in length of the acoustic canal. Results of the setup testing show maximal instantaneous temperature difference at the level of 0.5°C for the shorter, 300mm long acoustic canal (Fig. 14b). Data obtained for the longer, 400mm long canal (Fig. 15a and Fig. 15b) indicate essential drop in the obtained temperature difference, which corresponds to the numerical solution. The difference in particular values might come from limited data on the constructional features of the speaker, as well as the simplification on viscous boundary layer at the solid-gas interface, introduced within the selected environment [32].

Nevertheless, the results prove need for further experimental and numerical testing of the unit using high-porosity stack, with additional comparative analysis.

4. Conclusions

The discussed design strategy of the setup and its assumptions came from the fundamental physical theorem of the design and optimization of thermoacoustic devices, based on the fundamental acoustic and heat transfer laws. The performed computational analysis has proven the general correctness of the introduced design of the unit by indicating change in the essential operational parameters of the unit, following the change in its constructional features (the length of the resonator and the porosity of the stack). The results of the initial tests demonstrated the ability to observe the change in the selected operational parameters of the unit with the change in its configuration. Thereby, the criteria of simple parametric analysis were fulfilled. The experimental data corresponds to the values obtained from the numerical investigation, with the differences resulting from i.e. the inaccurate definition of the material properties of the stack and the limited data on the constructional features of the speaker.

Nevertheless, profound parametric analysis of the thermoacoustic devices, performing the role of refrigerators, characterized by different configurations, as well as further optimization of the setup, are required to introduce essential value to the future research.

Acknowledgements:

Authors acknowledge the financial support from the Silesian University of Technology through statutory research funds (grant number 08/050/BK_19/0186). Authors would like to thank Dr. Sebastian Michalski from Cranfield University for support during the initial design considerations.

Nomenclature

- a ambient speed of sound, $m \cdot s^{-1}$
- $A_{st,s}$ cross-sectional area of the stack occupied by the solid material, m^2
- $A_{st,w}$ cross-sectional area of the stack wetted by the working medium, m^2
- B stack porosity, dimensionless
- c_p specific heat capacity of the medium, $J \cdot kg^{-1} \cdot K^{-1}$
- k wavenumber, m^{-1}
- K thermal conductivity, $W \cdot m^{-1} \cdot K^{-1}$
- p_d dynamic pressure, Pa
- x average particle position, m
- x_d peak-to-peak particle displacement, m
- δ_a thermal penetration depth, m
- δ_v viscous penetration depth, m
- ω angular frequency of the wave, $rad \cdot s^{-1}$
- ρ density of the medium, $kg \cdot m^{-3}$

References:

[1] M.E.H. Tijani, J.C.H. Zeegers, A.T.A.M. de Waele: "Design of thermoacoustic refrigerators", *Cryogenics 42*, 49-57, 2002.

[2] G.W. Swift: "Thermoacoustic Natural Gas Liquefier", *US DOE Natural Gas Conference Proceedings*, Houston, 1997.

[3] B.L. Minner, J.E. Braun, L. Mongeau: "Optimizing the Design of a Thermoacoustic Refrigerator", *International Refrigeration and Air Conditioning Conference 1996*, 343.

[4] D.A. Russel, P. Weibull: "Tabletop thermoacoustic refrigerator for demonstrations", *Am J Phys 70*, 1231, 2002.

[5] A. Berson, M. Michard, P. Blanc-Benon: "Measurement of acoustic velocity in the stack of a thermoacoustic refrigerator using particle image velocimetry", *Heat Mass Transfer 44*, 1015-1023, 2008.

[6] T.D. Rossing (ed.): *Springer Handbook of Acoustics*, New York: Springer Science+Business Media LLC, 2007.

[7] K. Grzywnowicz, L. Remiorz: "Design of simple refrigerating device for multiparametric analysis of the thermoacoustic cooling phenomenon", in *ECOS 2019. Proceedings of the 32nd International Conference on Efficiency, Cost, Optimization, Simulation and Environmental Impact of Energy Systems*, Wroclaw, pp. 227-238, 2019.

[8] M.E. Poese, R.W. Smitth, S.L. Garrett, R. van Gerwen, P. Gosselin: "Thermoacoustic refrigeration for ice cream sales", *Proceedings of the 6th IIR Gustav Lorentzen Conference*, Glasgow, 2004.

[9] Kobayashi Y. et al.: "A unified stability analysis method for spontaneous oscillation conditions in thermoacoustic systems via measured frequency response data with application to standing- and traveling-wave engines", *J Sound Vib 456*, 86-103, 2019.

[10] Rulik S. et al.: "Influence of duct parameters on the acoustic wave generation", *Int J Numer Method H*, , doi: 10.1108/HFF-10-2018-0611.

[11] G. Harikumar et al.: "Thermoacoustic energy conversion in a square duct", *Enrgy Proced 158*, 1811-1816, 2019.

[12] R. Kikuchi et al.: "Measurement of performance of thermoacosutic heat pump in a -3 to 160 °C temperature range", *Jpn J Appl Phys* 54, 117101, 2015.

[13] M.E.H. Tijani,, S. Spoelstra: *High temperature thermoacoustic heat pump*, Energy Research Centre of the Netherlands, 2012.

[14] H.-B. Ke, Y.-W. Liu, Y.-L. He, Y. Wang, J. Huang: "Numerical simulation and parameter optimization of thermo-acoustic refrigerator driven at large amplitude", *Cryogenics 50*, 28-35, 2010.

[15] O.G. Symko, E. Abdel-Rahman, Y.S. Kwon, M. Emmi, R. Behunin: "Design and development of high-frequency thermoacoustic engines for thermal management in microelectronics", *Microelec J 35*, 185-191, 2004.

[16] I. Nowak et al: "Analytical and numerical approach in

the simple modelling of thermoacoustic engines", *Int J Heat Mass Tran 77*, 369-376, 2014.
[17]S.I. Zhu, G.Y. Yu, W. Dai, E.C. Luo, Z.H. Wu, X.D. Zhang: "Characterization of a 300 Hz thermoacoustically-driven pulse tube cooler", *Cryogenics 49*, 51-54, 2009.
[18]N.M. Hariharan, P. Sivashanmugam, S. Kasthurirengan: "Influence of stack geometry and resonator length on the performance of thermoacoustic engine", *Appl Acoust 73*, 1052-1058, 2012.
[19]S. Spoelstra: *THermoAcoustic Technology for Energy Applications. Final Report*, Energy research Centre of the Netherlands, Petten, 2012.
[20]P. Lotton, P. Blanc-Benon, M. Bruneau, V. Gusev, S. Duffourd, M. Mironov, G. Poignand: "Transient temperature profile inside thermoacoustic refrigerators", *Int J Heat Mass Tran 52*, 4986–4996, 2009.
[21]S. Michalski, K. Grzywnowicz, L. Remiorz: „Thermoacoustic cooling phenomenon - test stand conception*", Rynek Energii 133*, 73-79, 2017.
[22]Tijani M.E.H. (2001). *Loudspeaker-driven thermo-acoustic refrigeration* (Doctoral dissertation), Technische Universiteit Eindhoven, Eindhoven.
[23]A.C. Alcock, L.K. Tartibu, T.C. Jen: "Experimental investigation of an adjustable thermoacoustically-driven thermoacoustic refrigerator", *Int J Refrig 94*, 71-86, 2018.
[24]A.A. Rahman, X. Zhang: "Single-objective optimization for stack unit of standing wave thermoacoustic refrigerator through fruit fly optimization algorithm", *Int J Refrig 98*, 35-41, 2019.
[25]P. Yehui, F. Heying, M. Xiaoan: "Optimization of standing-wave thermoacoustic refrigerator stack using genetic algorithm", *Int J Refrig 92*, 246-255, 2018.
[26]K. Kuzuu, S. Hasegawa: "Effect of non-linear flow behavior on heat transfer in a thermoacoustic engine core", *Int J Heat Mass Tran 108*, 1591-1601, 2017.
[27]L. Qiu, B. Wang, D. Sun, Y. Liu, T. Steiner: "A thermoacoustic engine capable of utilizing multi-temperature heat sources", *Energ Convers Manage 50*, 3187-3192, 2009.
[28]P. Saechan, A.J. Jaworski: "Numerical studies of co-axial travelling-wave thermoacoustic cooler powered by standing-wave thermoacoustic engine", *Renew Energ 139*, 600-610, 2019.
[29]Visaton GmbH "Visaton K40 - 8 Ohm product card", Haan: Visaton – 2015.
[30]Euratech "ABS Material Eurapipe Duraflo product card" Nilay: Euratech, , 2017.
[31]K. Rogoziński, I. Nowak, G. Nowak: "Modeling the operation of a thermoacoustic engine", *Energy 138*, 249-256, 2017.
[32]B. Ward, J. Clark, G. Swift: *Design Environment for Low-amplitude Thermoacoustic Energy Conversion DeltaEC Users Guide*, Los Alamos National Laboratory, Los Alamos 2016.